The Folded Horn Antenna

Everett G. Farr and Leland H. Bowen
Farr Research, Inc.

Carl E Baum
University of New Mexico

William D. Prather
Air Force Research Laboratory / DE

Abstract

Antennas for radiating high-power mesoband electromagnetic signals are critical to the mission of upsetting electronics at a distance. High Power Microwave (HPM) weapons require efficient antennas that can fit into a small volume. Many of the existing antennas, such as pyramidal horns, are too large to fit onto many platforms when operated at low frequency. To address this problem, we investigate the folded horn, which has aperture dimensions of 0.5 X 2 wavelengths, and a depth of 1.5 – 2 wavelengths. This antenna has a nearly focused aperture field, due to a parabolic fold in the H-plane. We built and tested a folded horn at 3 GHz. We found a gain of 10 dB, an aperture efficiency of 80%, and a bandwidth that ranged from 3-5 GHz. This design could be adapted to high-voltage designs, and it could work well in a dual-antenna configuration, with two antennas positioned back-to-back, driven by a dual-output source. It may also be applicable to other applications and frequency ranges.

CONTENTS

I. Introduction

Folded horn antennas have recently been proposed by C. E. Baum for radiating high-power mesoband signals from a very compact package with high efficiency and moderate gain [1]. These antennas are shorter than pyramidal horns, so they can fit into smaller spaces. These devices were intended to operate at a frequency of a few hundred megahertz, and they were intended for the application of upsetting electronics at a distance. Beyond this rather narrow application, folded horns may also be useful at other frequencies and in other applications that demand reasonable gain out of an antenna with a compact package.

In this paper, we build and test the first prototype low-power folded horns, operating at a center frequency of 3 GHz. We describe several iterations, resulting in a design that satisfies our requirements over 3-5 GHz. We also describe alternative configurations, and we suggest further improvements that could result in improved performance and/or a more compact size. We begin now with a description of the folded horn.

II. Folded Horn Description and Analysis

A. Description

The original sketch of the folded horn, as proposed by C. E. Baum, is shown in Figure 2.1 This device consists of three parts: the Feed Section, the Parabolic Bend, and the Aperture Section. When operating at its center frequency, this antenna has an aperture of 0.5 X 2 wavelengths, and a depth of around 1.5 – 2 wavelengths.

The folded horn works as follows. The feed point and switch are located in the Feed Section, in which the horn is expanded in the H-plane. A cylindrical wave is launched from the feed point, which is positioned at the focus of the parabolic bend. After reflecting off the parabolic bend, the waves are focused in the H-plane and then proceed into Aperture Section, in which the fields are expanded in the E-plane. The fields in the large dimension of the aperture (H-plane) remain focused, because of the parabolic bend. The fields in the short dimension of the aperture (E plane) are only slightly out of focus, because there is little difference in ray path lengths in this plane. In the next section, we calculate the degree of defocus in the E-plane.

If one were operating at high voltage, one could stack a second folded horn on top of the first, as shown in Figure 2.2, allowing both systems to share a single switch, effectively doubling the output voltage.

If one had to radiate a high-power mesoband signal, one might compare the folded horn to a half Impulse Radiating Antenna, which is currently used. The folded horn has a number of advantages over a half IRA in mesoband applications. In the folded horn there is no spillover, because the horn fills the aperture. The fields are spread uniformly across the aperture, without sharp spikes near the feed arms. And there is room for two sources and antennas within the same volume that would normally be taken up by a half IRA.
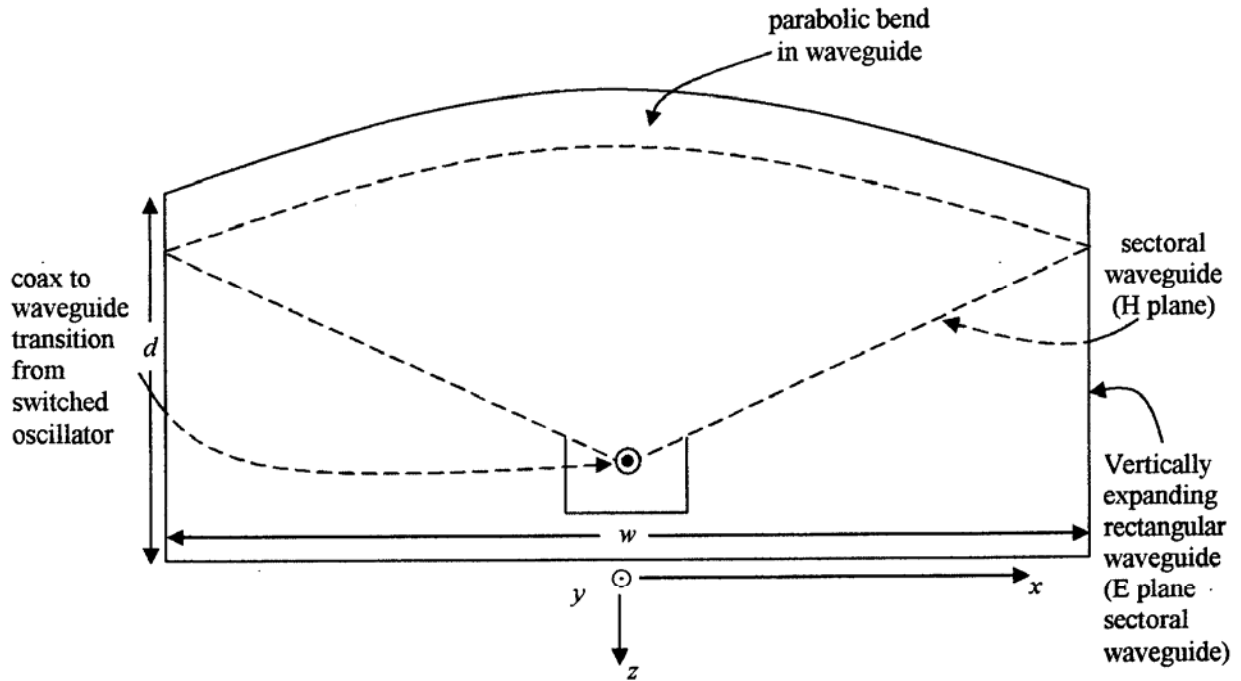
A. Top View
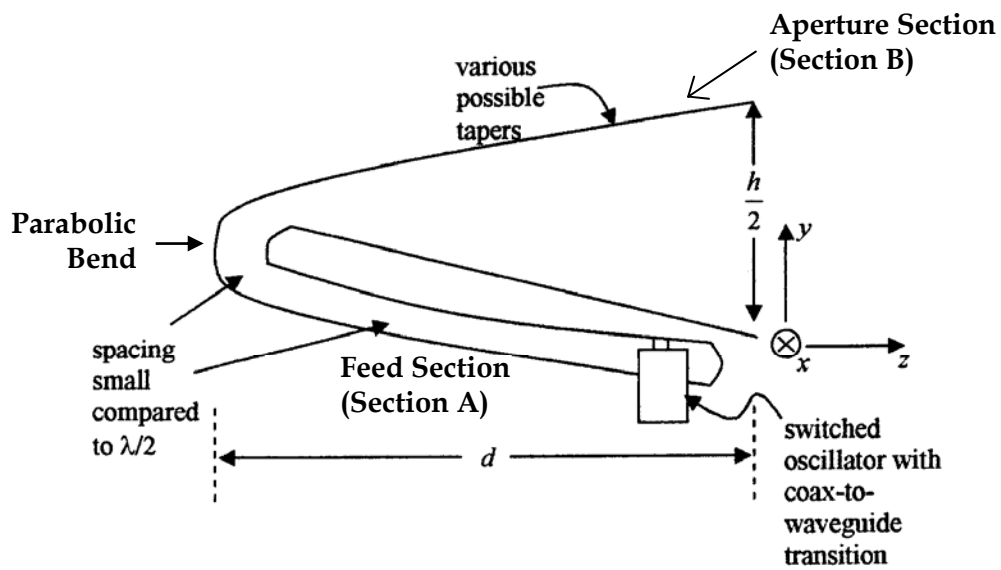
B. Side view (cross section)

Figure 2.1. The Folded Horn, showing a switched oscillator feed, a parabolic bend, from [1].
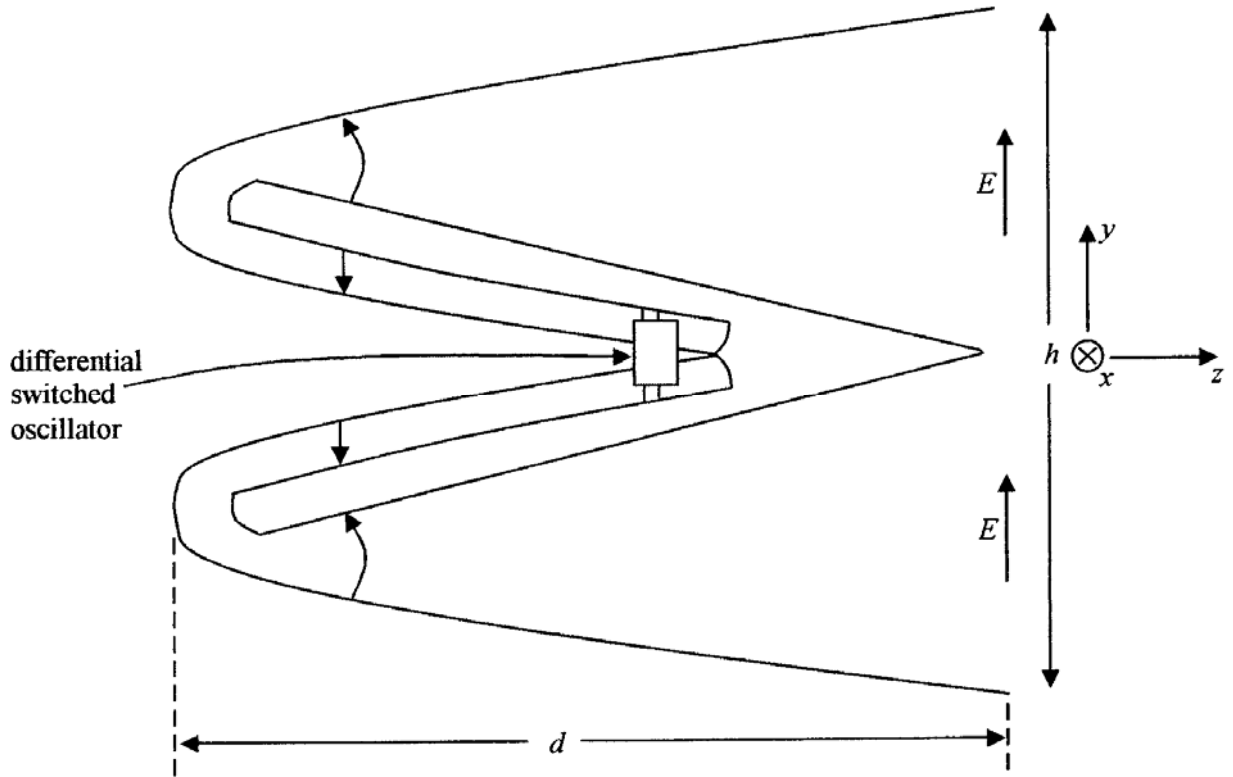
Figure 2.2. Two Folded Horns in a back-to-back configuration with a differential feed, from [1].

B. Analysis

We describe here the aperture fields in the folded horn, and we calculate the radiated far fields on boresight for the folded horn. We design an antenna with an aperture of 0.5 X 2 λ, and with a depth of ¾ λ.

A sketch of the aperture electric fields of the folded horn appears in Figure 2.3. On the left, we see that the electric fields protrude slightly from the aperture, due to a slight defocus in the E-plane. On the right, we observe that the electric field varies as a sine function across the aperture, because of the metal walls on either side.
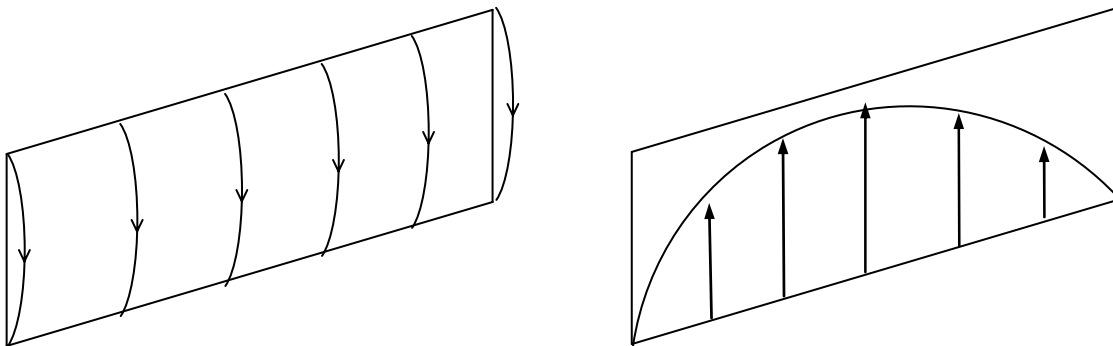
Figure 2.3. Aperture electric fields of the folded horn.

We begin the analysis by calculating the level of defocus in the aperture fields. We do so by calculating the path length difference between a central ray and an extreme ray. In Figure 2.4 we see a cut through the Aperture Section of the folded horn. By the Pythagorean theorem, the extreme ray has a length of 0.79 λ, compared to a direct path length of 0.75 λ, resulting in a path length difference of 0.04 λ. We believe that such a short path length difference will avoid significant defocus. So the aperture is essentially in focus.
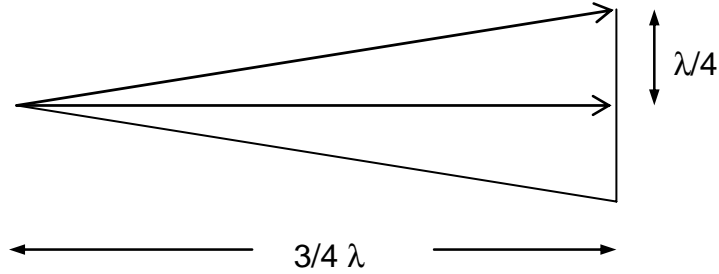
Figure 2.4. Geometry for calculating the level of defocus in the folded horn Aperture section.

Radiated Fields of Folded Horn

Next, we calculate the field radiated from a folded horn with aperture size of 0.5 X 2 λ. We begin by calculating the gain available in the folded horn. Thus,

$$G = e \frac{4\pi}{\lambda^2} A \qquad (2.1)$$

where A is the aperture area, λ is the wavelength, and e is the aperture efficiency. Because of the sinusoidal field distribution, $e = 0.81$, according to [1]. For this aperture, $A = \lambda^2$, so we have $G = 0.81 (4\pi) = 10.2$. Thus, for a single folded horn we have

$$G = 10.2 = 10.1 \, \text{dB} \qquad (2.2)$$

at the design frequency.

Next, we calculate the radiated field from a folded horn. The radiated power density is

$$S = \frac{G P_{in}}{4\pi r^2} \qquad (2.3)$$

where P_{in} is the power accepted into to the antenna. Using $P_{in} = V_o^2/Z_c$, where Z_c is the input impedance, and $S = E_{rad}^2/\eta$, where $\eta = 377 \, \Omega$, we simplify to find.

6

$$\frac{r\,E_{rad}}{V_o} = \sqrt{\frac{\eta}{Z_c}\frac{G}{4\pi}} \qquad (2.4)$$

If we assume that the input impedance is 50 Ω, then we have for a single folded horn,

$$\frac{r\,E_{rad}}{V_o} \approx 2.5 \qquad (2.5)$$

for a single antenna. If we drive two of these antennas with equal-but-opposite sources as shown in Figure 2.3, the total normalized radiated field is doubled, so

$$\frac{r\,E_{rad}}{V_o} \approx 5 \qquad (2.6)$$

for the dual folded horn with dual sources triggered by a single switch.

III. FH-1: The First Folded Horn

We selected for initial experiments the design shown in Figure 3.1, designated FH-1. This antenna is designed to operate at 3 GHz, which gives a wavelength of $\lambda = 0.1$ m; so the aperture is 0.05 X 0.2 m (0.5 X 2 λ). This makes the antenna small enough to allow easy construction and testing.

The FH-1 was designed so it could be constructed entirely from flat pieces of sheet metal. In cases where curved parts were required, they were shaped from flat pieces by bending in a single plane of curvature. We show the flat patterns for the parts in Figure 3.2. The parts were cut from 20 Ga. brass and, in most cases, soldered together to form the folded horn. In locations where soldering could warp the metal, we used copper tape.

In addition to the FH-1 antenna, we also built a separate feed section called FH-1-FS, shown in Figures 3.3 and 3.4. Having a separate feed section allowed us to make a number of measurements that otherwise would not have been possible. It allowed us to make measurements on both the feed section and the complete antenna during a single test. It also allowed us to more simply investigate various feed point geometries, without installing them in the complete antenna. Finally, it allowed us to investigate how well the fields filled the full 139° angle of the feed section. Note that the feed point is located at the center of the circular section, which is also the apex of the horn and the focus of the parabolic bend.

A number of features near the feed point require clarification. The radius of the pill box surrounding the feed point was $\lambda/4$ at the design frequency, 3 GHz. This was chosen so the short circuit at the edge of the pill box would look like an open circuit at the feed. In addition, the feed point consisted simply of extending the center conductor of the SMA female connector all the way through the cavity. Later in this paper we refine this geometry.

7
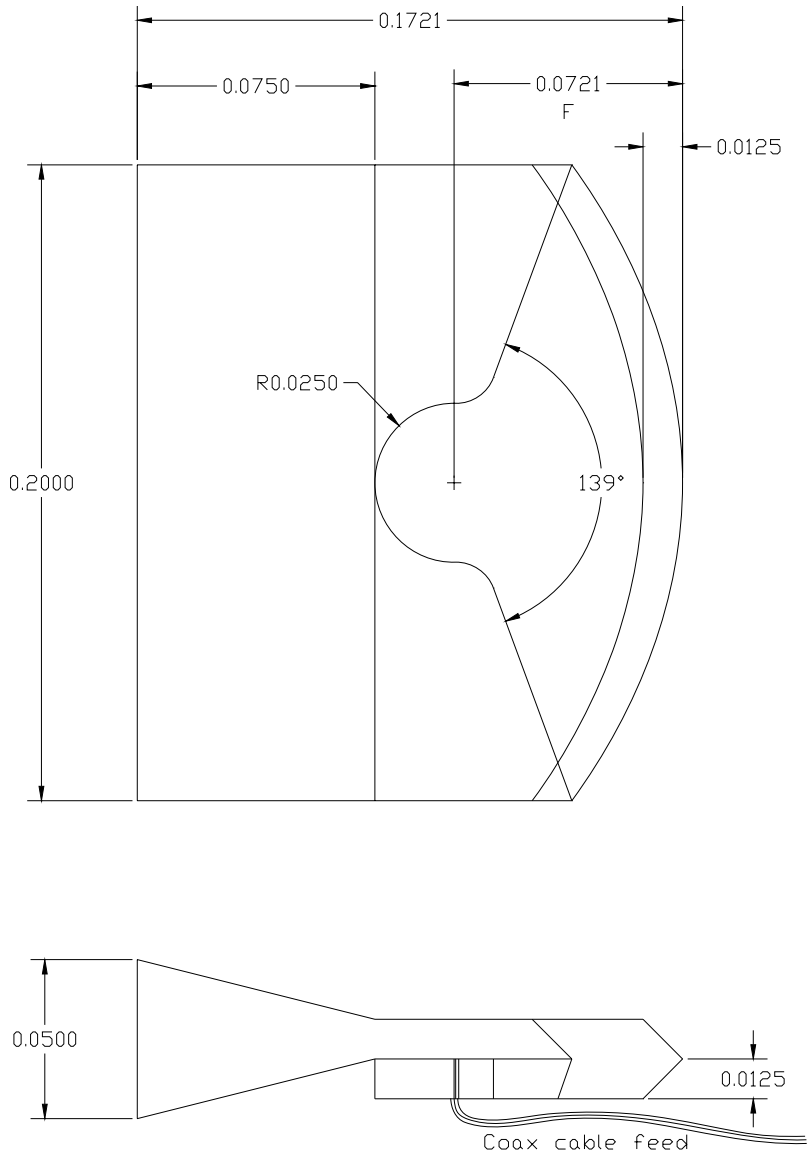
Figure 3.1. FH-1 drawing. Dimensions are in meters.
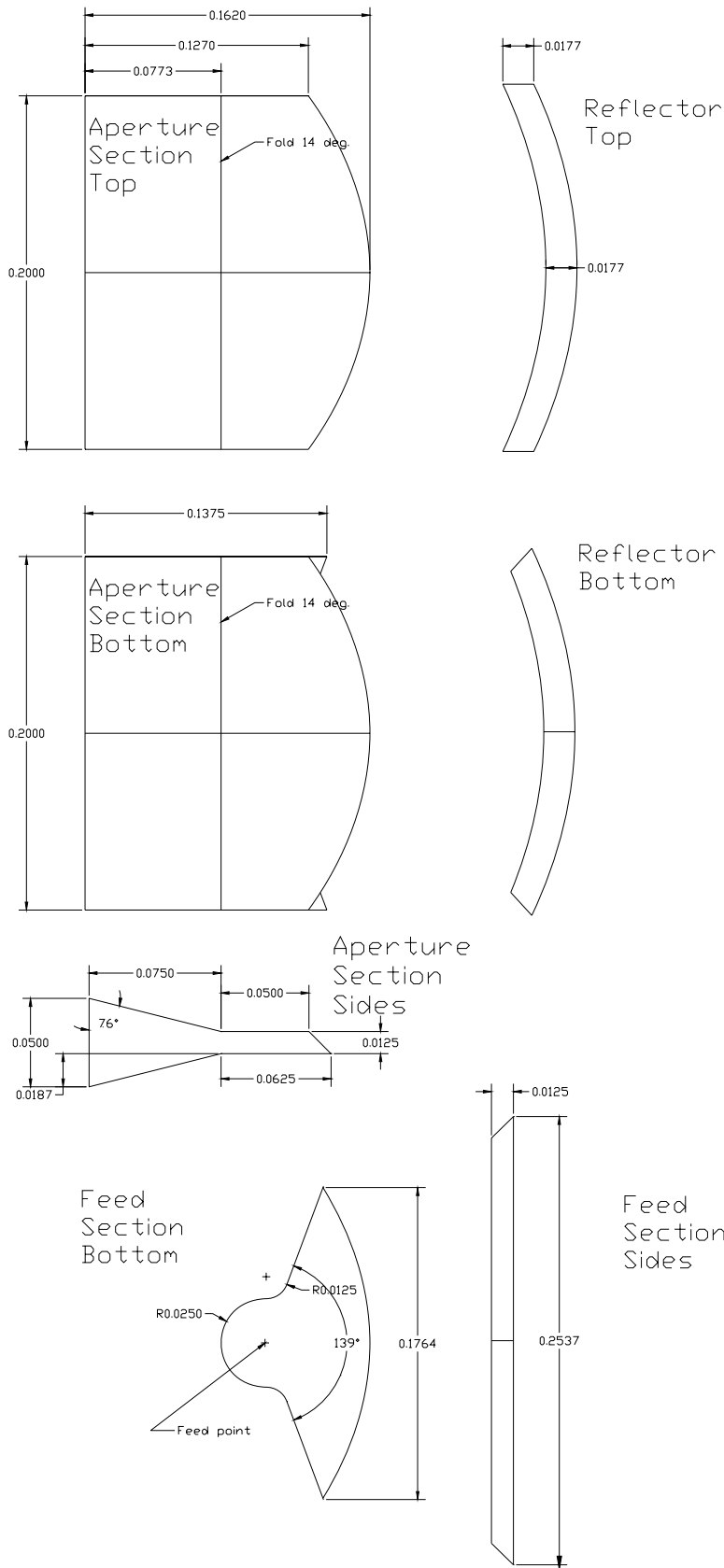
Figure 3.2. Patterns for FH-1 parts. Dimensions are in meters.

Figure 3.3. Bottom view of the FH-1-FS showing the SMA connector at the feed point.
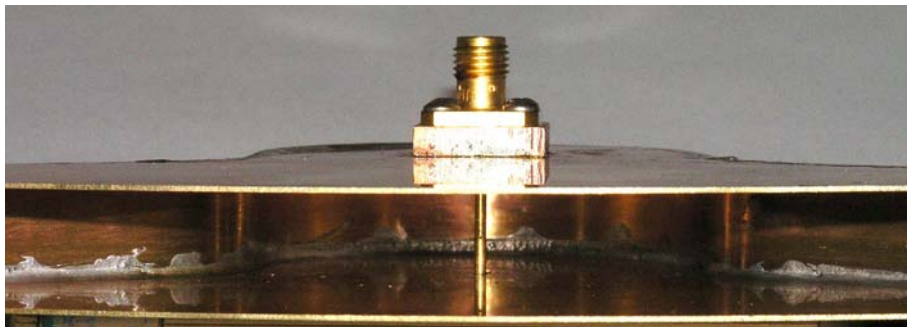
Figure 3.4. Inside view of feed section.

The shape of the bend also requires some clarification. We wanted to keep the entire feed section within the $\lambda/2$ height of the aperture, and this goal was particularly challenging to meet. We had to implement a 180-degree bend in the waveguide at the parabolic bend, and there was little room to implement it. The height of the waveguide was $\lambda/8$ in the feed section. In order to make the 180-degree bend within the available space, we built two 45-degree reflectors, as shown in Figure 3.5. The dotted arrows show the path of a typical ray. With this configuration, all rays have the same path length around the bend, which is necessary to keep the wavefront in focus. Note that the knife-edge in the center may have to be rounded off when operating at higher powers.
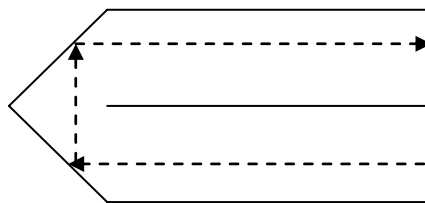
Figure 3.5. Detail of the 180-degree bend.

In Figure 3.6 we show two views of the complete folded horn (FH-1). The feed section (FH-1-FS) can be seen on the bottom of the aperture section in the picture on the right. The feed section can also be seen in Figure 3.7, where we show a larger view from the back to show the parabolic reflector. The two halves of the reflector were soldered together and then attached to the folded horn with copper tape.
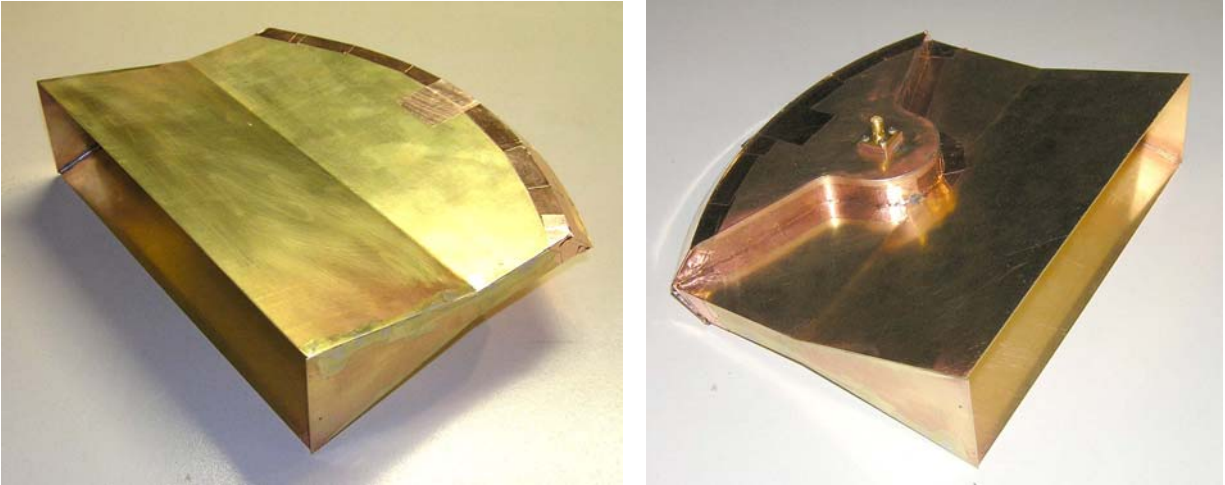
Figure 3.6. Top and bottom views of the FH-1.
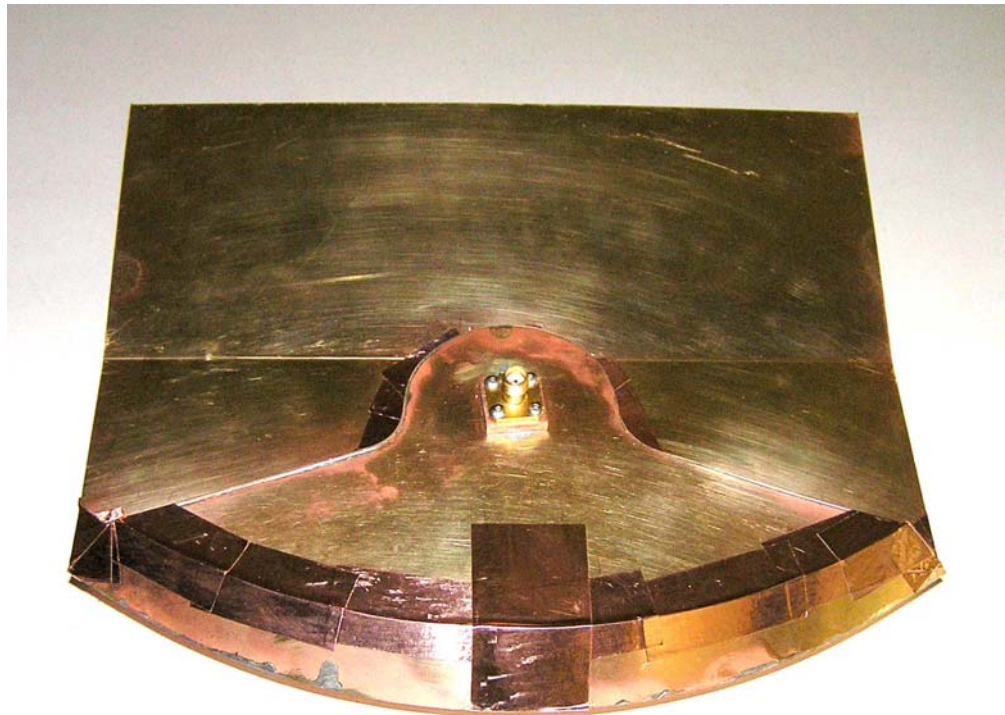
Figure 3.7. Enlarged view of the bottom of the FH-1 showing the reflector section.

IV. Characterization of the FH-1-FS and FH-1.

We provide here a complete set of antenna data for the first version of the folded horn feed section, FH-1-FS, and for the complete folded horn, FH-1.

All data were acquired on our *PATAR*[TM] time domain antenna range. The source for this system is a Picosecond Pulse Labs model 4015C step generator, which drives a Farr Research model TEM-1-50 sensor. The 4015C is a high-speed pulser with a negative 4 V voltage step, with a fall time of 20 ps. The antenna under test (AUT) was placed 4 m from the aperture of the TEM sensor. The output of the AUT was recorded using a Tektronix model TDS8000 sampling oscilloscope with an 80E04 sampling head.

In Figures 4.1-4.3, we show the results for the feed section. The TDR and S_{11} are shown in Figure 4.1, boresight gain is shown in Figure 4.2, and pattern data is shown in Figure 4.3. In the TDR we observe a very large impedance spike at the feed point, which is clearly undesirable. Furthermore, the dip in S_{11} shows that the antenna operates best at 5.5 GHz, which is much higher than the design frequency of 3 GHz. In the next section, we investigate a variety of feed-point modifications designed to address these problems.

One reason for testing the feed section separately was that this allows us to investigate how well the electric fields fill the antenna in the H-plane. The dimensions of the feed section expand in the H-plane at an angle of 139° (±70°), and there was some concern that the field might not completely fill such a large angle. We tested this by measuring the antenna pattern of the feed section by itself, shown in Figure 4.3. We see the pattern is quite broad in the H-plane, and the field drops to zero at the edges of this expansion section (±70°), as it should. The pattern in the E plane is nearly flat as one might expect, since the feed section is very narrow in this direction. So we conclude that the field does fill the entire 139° angle of the feed section.

In Figures 4.4-4.6 we show the results for the complete folded horn (FH-1). We observe that the S_{11} has a minimum value near 6 GHz, which is close to the 5.5 GHz observed when looking just at the feed section. This is an important result, because it suggests that characteristics of the isolated feed section provide a good estimate of the S_{11} of the overall antenna. We experiment with a number of feed configurations in the following section, and it is much simpler to conduct experiments on the isolated feed section than on the entire antenna.

In the next section, we consider a number of methods of improving the feed point design.

12
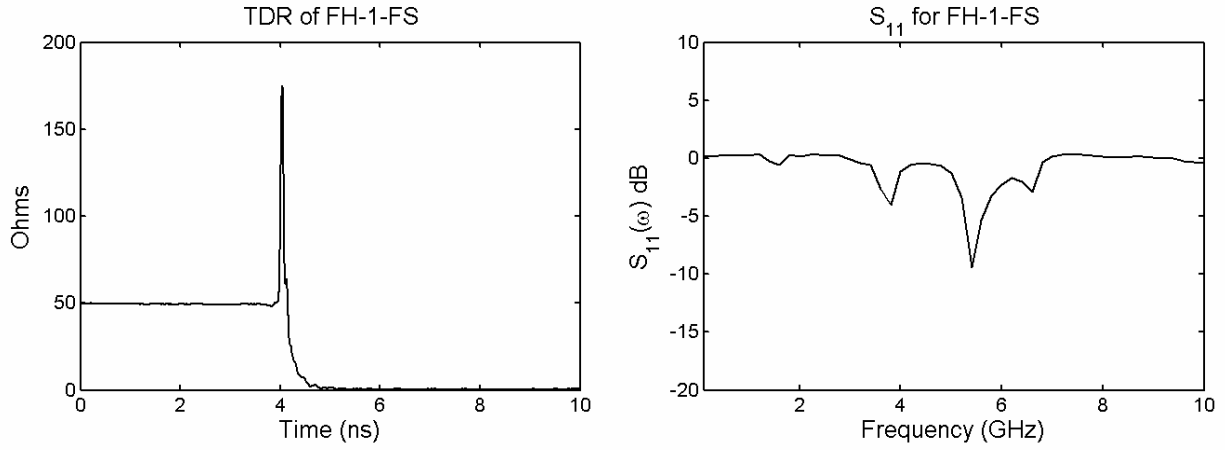
Figure 4.1. TDR and S_{11} of FH-1-FS feed section.
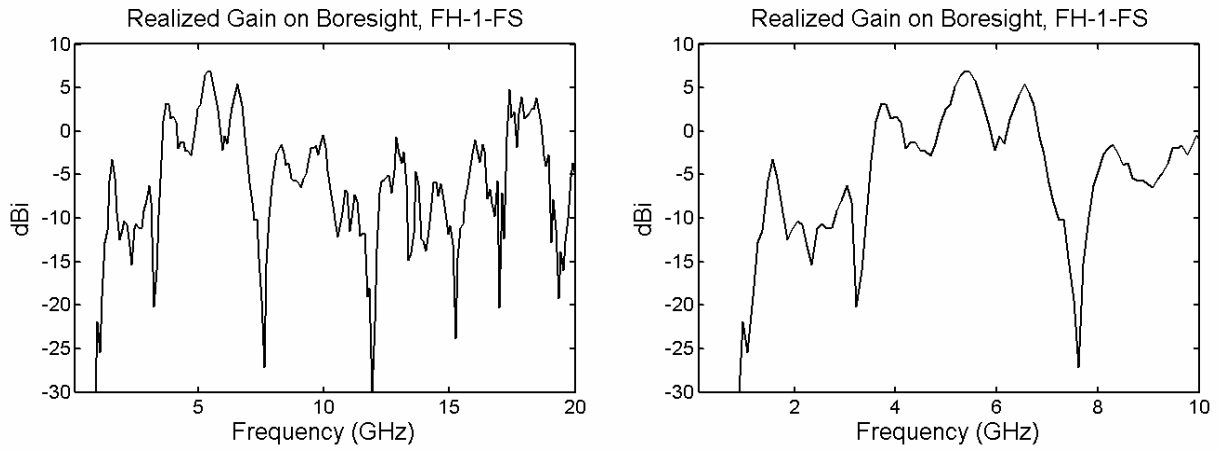
Figure 4.2. Realized Gain of FH-1-FS feed section.
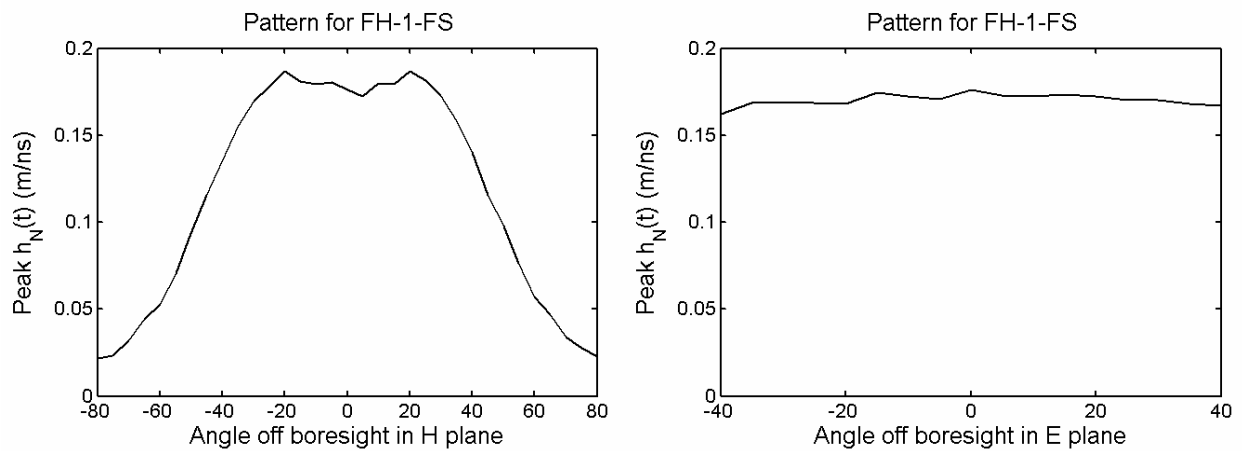
Figure 4.3. Antenna pattern for FH-1-FS feed section.
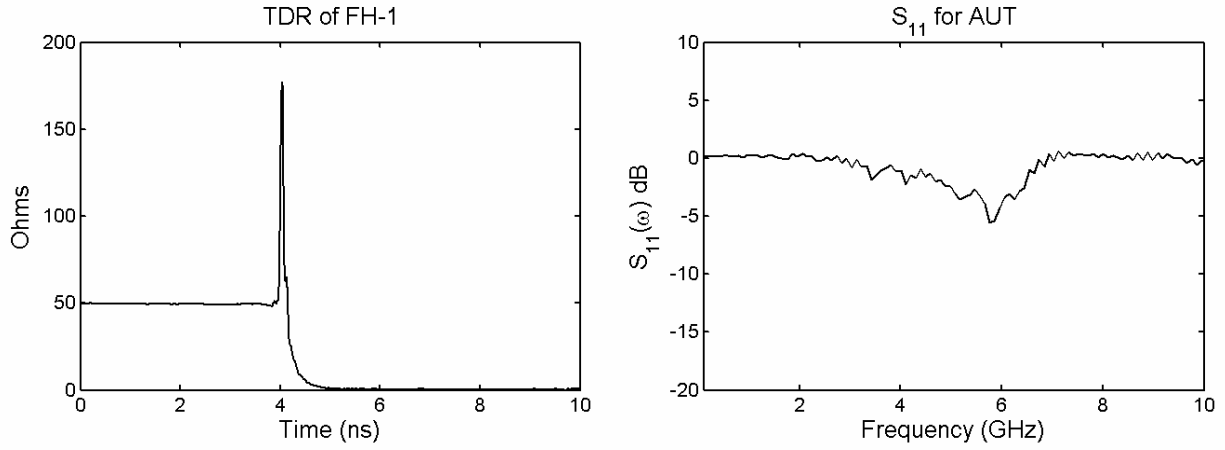
Figure 4.4. TDR and S_{11} of FH-1 folded horn.
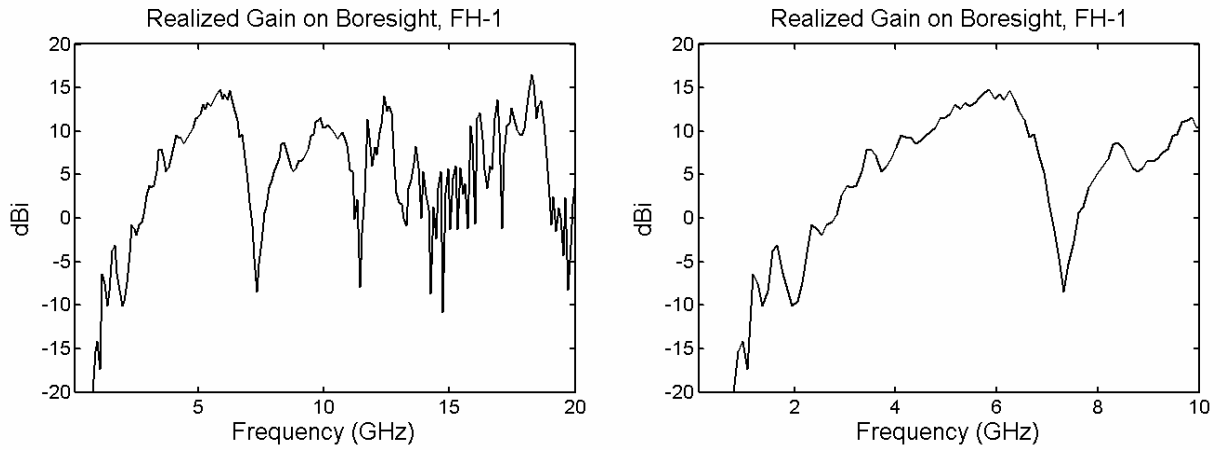
Figure 4.5. Realized Gain of FH-1 folded horn.
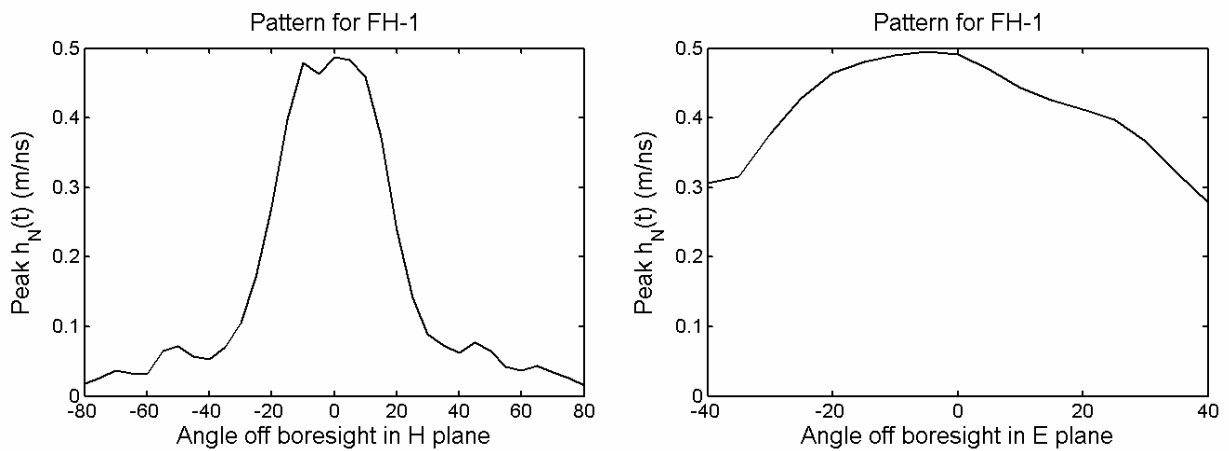
Figure 4.6. Antenna pattern for FH-1 folded horn.

V. Feed Section Modifications

The first version of the folded horn performed best at a frequency significantly higher than desired. To address this problem, one might increase the antenna size, but that would defeat the purpose of building an electrically small antenna with moderate gain. Thus, we investigate a number of modifications to the feed point in an attempt to lower the operating frequency.

For our first feed point modification, we filled the pill box at the feed point with a cylindrical Teflon disk, with a dielectric constant of about 2.0. A photo of the Teflon disk is shown in Figure 5.1. The intent here was to make the feed point region electrically larger, which should lower the operating frequency. At high voltages, the volume near the feed point will have to be filled with oil anyway, so adding a Teflon disk is a reasonable approximation. Note that our pill box has a radius of $\lambda/4$ in air at 3 GHz.

The resulting TDR and S_{11} are shown in Figure 5.2, where we observe that the spike in TDR at the feed point is significantly reduced. Furthermore, the S_{11} shows a significant dip near 3 GHz, which was quite encouraging, but clearly left some work to be done.
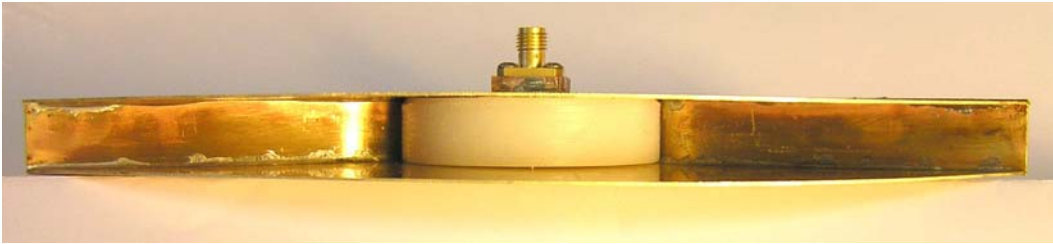
Figure 5.1. FH-1-FS-A with Teflon disk.
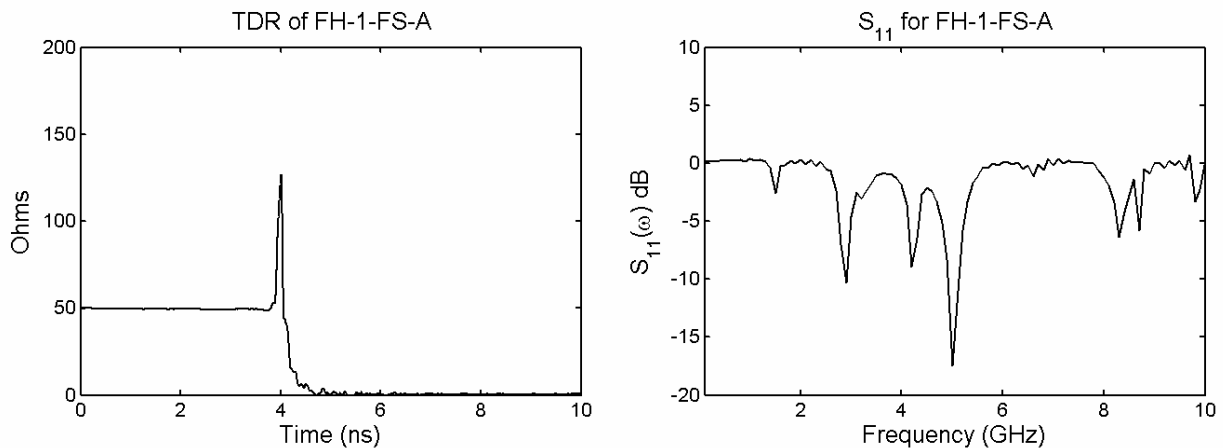
Figure 5.2. TDR and S_{11} of FH-1-FS-A, with Teflon disk.

In our second feed point modification, we shortened the center pin of the SMA connector so it extended only halfway across the waveguide, as shown in Figure 5.3. This was motivated by observing a standard coax-to-rectangular waveguide adapter, which has a pin that goes only

halfway across the waveguide. The TDR and S_{11} of this configuration are shown in Figure 5.4, where we see the shortened pin causes the impedance to quickly jump to infinity at the feed point due to the open circuit. The S_{11} for this version was similarly not very good. Next, we tried adding the Teflon disk with the shorter pin, resulting in the TDR and S_{11} shown in Figure 5.5. The S_{11} for this case has been improved a bit, but it is still very poor.
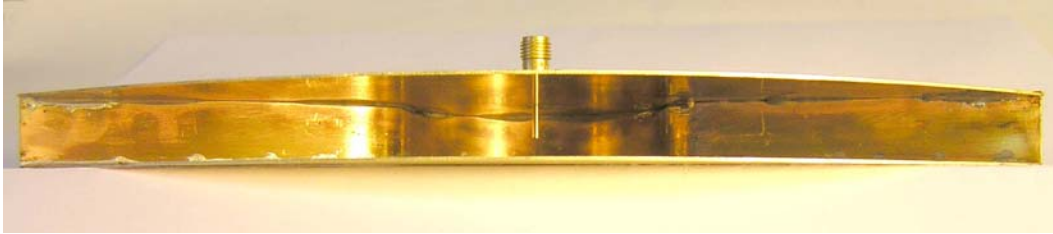
Figure 5.3. FH-1-FS-B with short feed conductor.
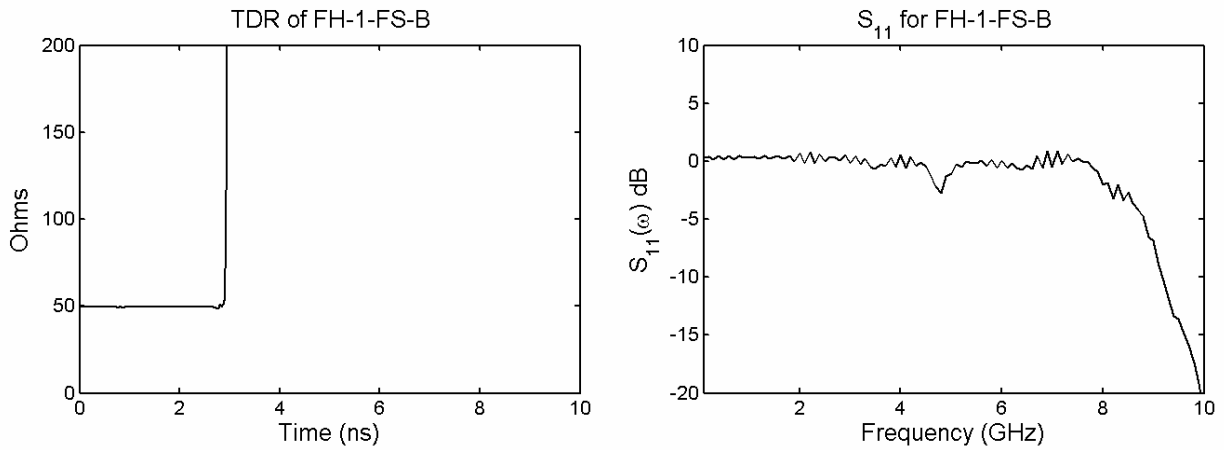
Figure 5.4. TDR and S_{11} of FH-1-FS-B feed section, with short feed wire.
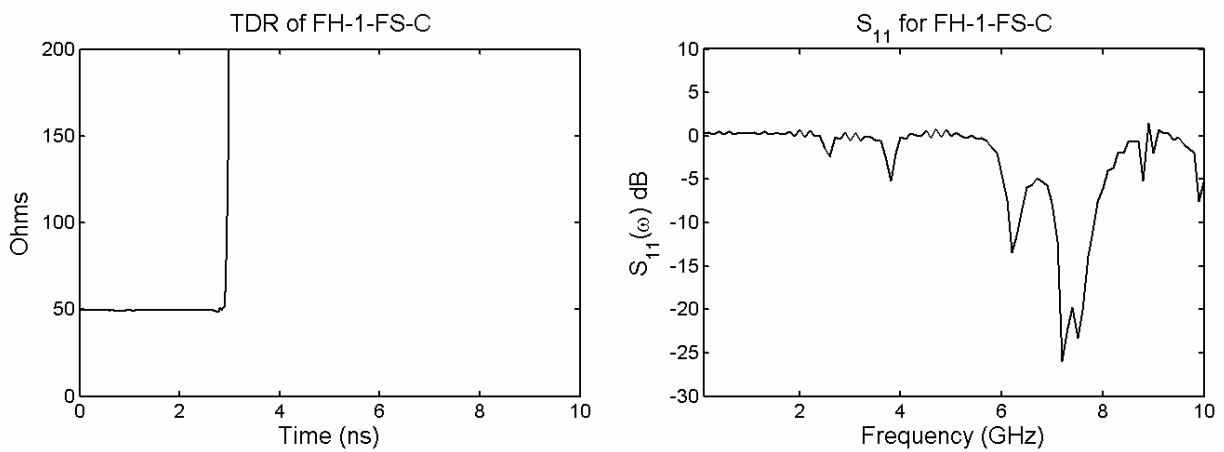
Figure 5.5. TDR and S_{11} of FH-1-FS-C feed section, with short feed wire and Teflon disk.

The next feed point modification we tried was to make the feed pin to look like a 50 Ω conical transmission line over a ground plane. It was thought that this would reduce the impedance spike shown previously in Figure 4.1. At first, no Teflon disk was used.

The impedance of a cone against a ground plane in free space is [2]

$$Z_o = \frac{\eta}{2\pi} \ln(\cot\theta_h / 2) \tag{5.1}$$

where $\eta = 377$ Ω is the impedance of free space, and θ_h is the half-angle of the cone. To realize a 50-Ω impedance, $\theta_h = 47^o$, so the total included angle of the cone should be 94°. We had a handy method available of generating a cone with total included angle of $62.4°$, so we tried that first, realizing that the impedance would be a little high, 77 Ω.

We provide a photo of the cone at the feed point in Figure 5.6. The TDR for this configuration, shown in Figure 5.7, shows a much reduced impedance spike at the feed point. In Figure 5.7 we also see that the S_{11} was significantly improved, and that the antenna now operates at a lower frequency.

Finally, we added the Teflon disk to the cone, in an attempt to lower the operating frequency even further. This was implemented in a rather crude manner, using a standard counter sink (82° total included angle) to make an opening in the disk for the cone. This left a small air gap that is largest at the apex. We used the same cone as in the previous version, resulting in an impedance of 54 Ω, not accounting for the air gap. We expect to use more precise machining in later projects, when more time is available.

Results with the conical feed point and Teflon disk are shown in Figure 5.8. The spike in the TDR is nearly gone now, and there is a nice dip in the S_{11} near 3 GHz. Thus, we have made substantial progress beyond our original design.

Since the cone and Teflon disk provided the best performance in the feed section, we added them to the complete folded horn, as described in the next section.
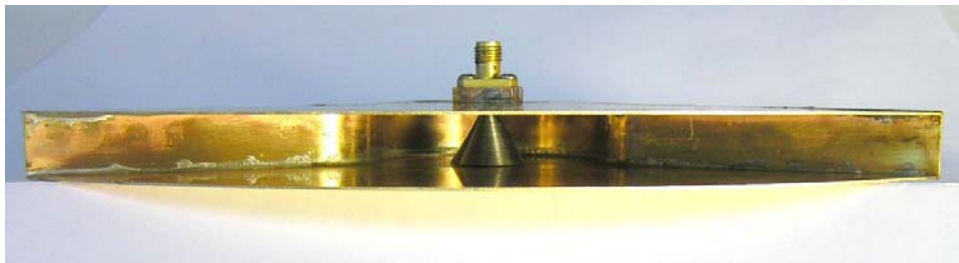
Figure 5.6. FH-1-FS-D with conical feed.
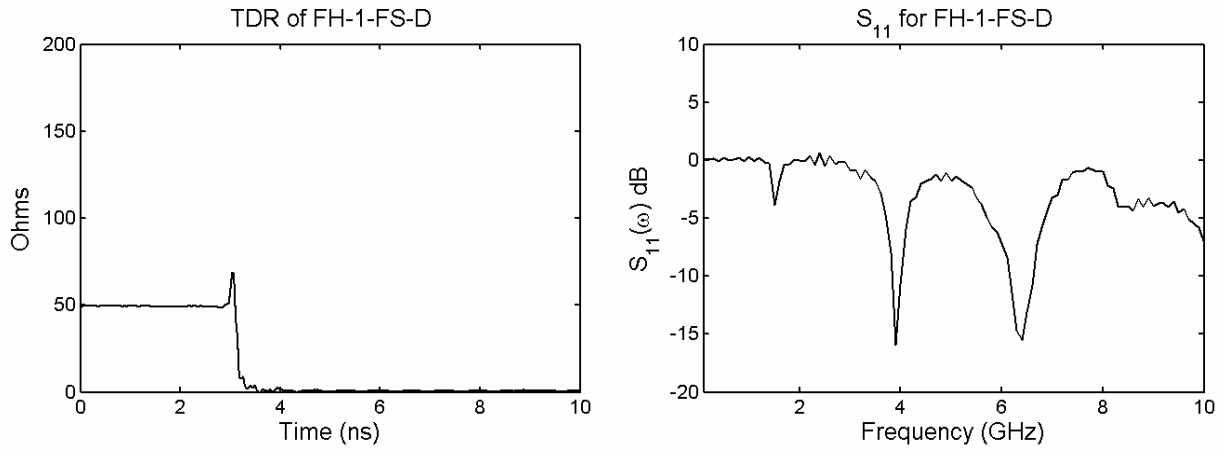
Figure 5.7. TDR and S_{11} of FH-1-FS-D with conical feed.
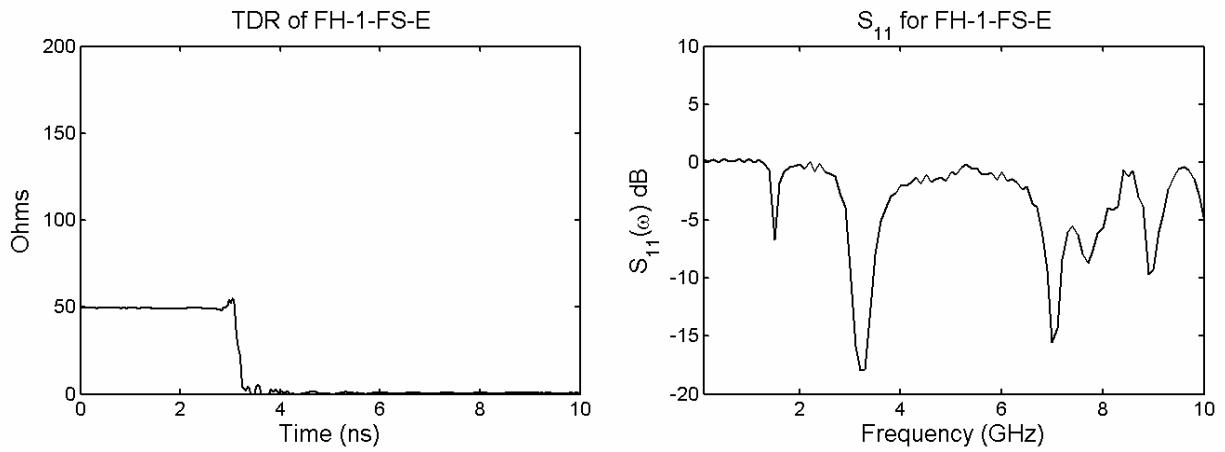
Figure 5.8. TDR and S_{11} of FH-1-FS-E with conical feed and Teflon disk.

VI. Characterization of the FH-1E

Next, we added the cone and Teflon disk to the complete antenna, resulting in a folded horn we call FH-1E. We provide here a complete set of data for the FH-1E, beginning with the TDR and S_{11} for the FH-1E, shown in Figure 6.1. The TDR is quite smooth at the feed point, and the S_{11} has a nice dip near 3 GHz, which is consistent with earlier measurements of the feed section

The realized gain on boresight is plotted in Figure 6.2. The realized gain is 10 dB or better over a frequency range of 3-5 GHz. This is quite impressive performance for such a small antenna, as we will see when we compare it to related designs later in this report.

The antenna patterns in the H and E planes are shown in Figure 6.3. These patterns are based on realized gain normalized to boresight. We see that the H-plane pattern is much narrower than the E-plane pattern, as we expect. We also provide polar antenna patterns at selected frequencies, as shown in Figure 6.4. These plots allow one to observe the change in beamwidth with frequency.

Based on the above results, we can estimate the aperture efficiency of the folded horn at its design frequency of 3 GHz. It has a gain of 10 dB = 10 (absolute) with an aperture area of 2λ X $\lambda/2 = \lambda^2$. Referring back to equation (2.1), we know everything except the aperture efficiency, which we find to be 80%. This is consistent with our original prediction of an aperture efficiency of 0.81, and a gain of 10.1 dB, as calculated in equation (2.2). We consider this to be an impressive result for our first attempt. This is also consistent with our original prediction of an aperture efficiency of 0.81, and a gain of 10.1 dB, as calculated in equation (2.2). So we are quite close to the expected result.
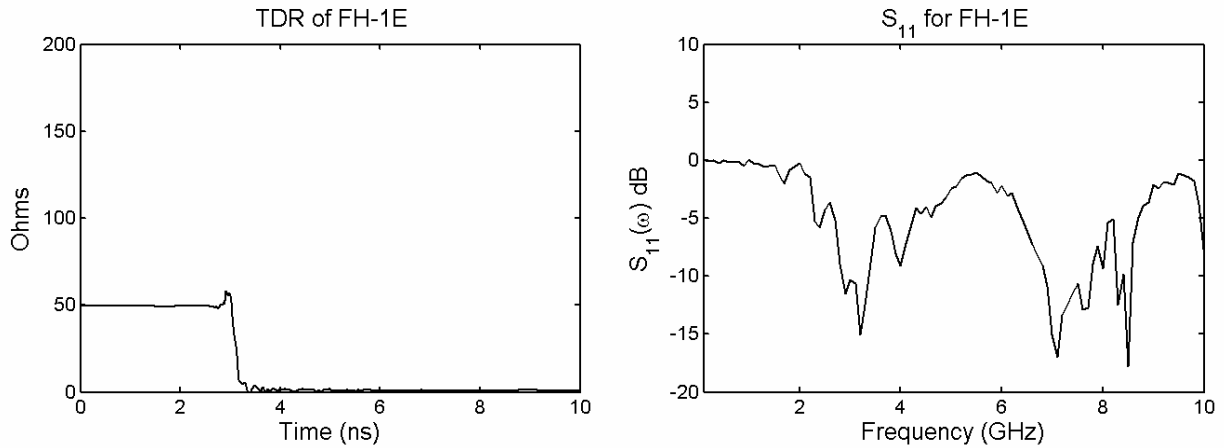
Figure 6.1. TDR and S_{11} of FH-1E with conical feed and Teflon disk.
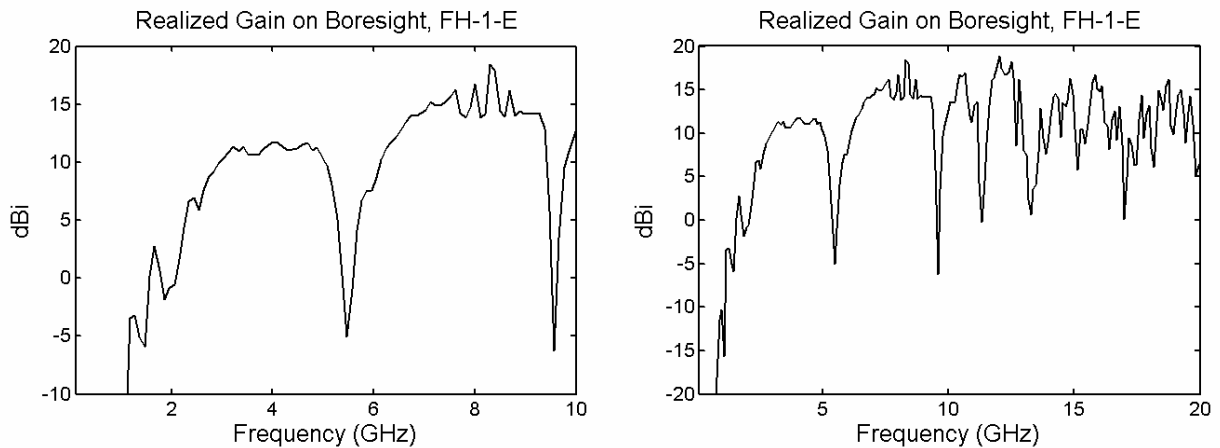
Figure 6.2. Realized gain of the FH-1E with conical feed and Teflon disk.
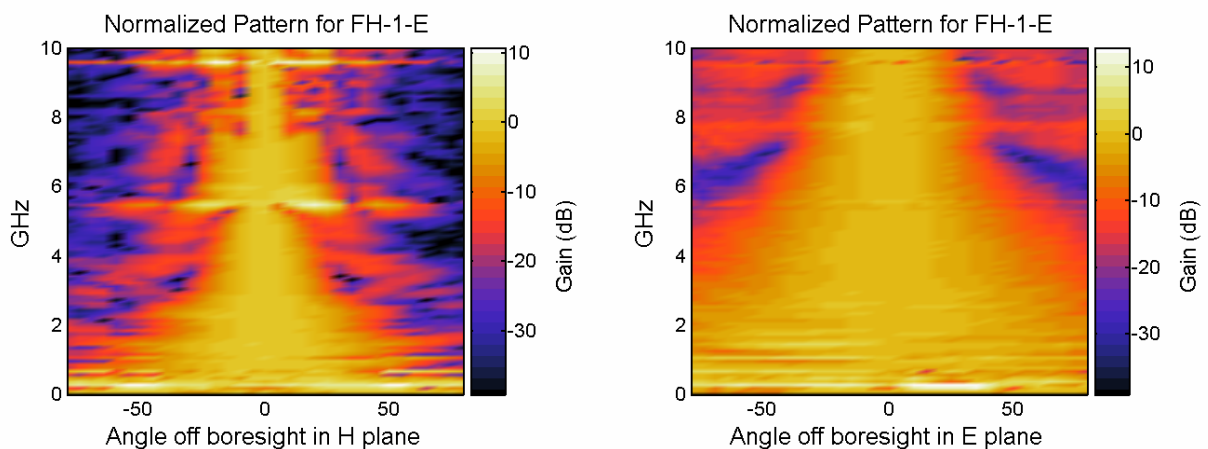
Figure 6.3. Normalized pattern as a function of frequency for the FH-1E, based on realized gain normalized to boresight.

Realized Gain at 1000 MHz, FH-1E
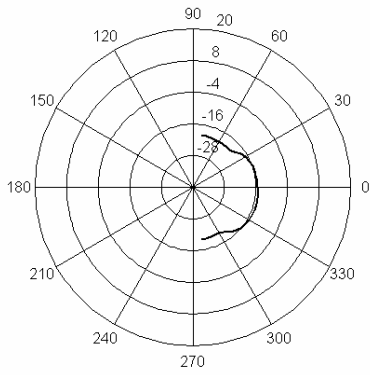
Azimuth (H plane)

Realized Gain at 1000 MHz, FH-1E
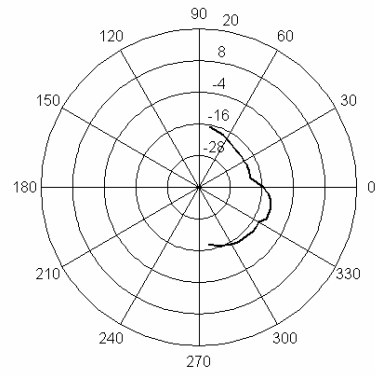
Elevation (E plane)

Realized Gain at 2000 MHz, FH-1E
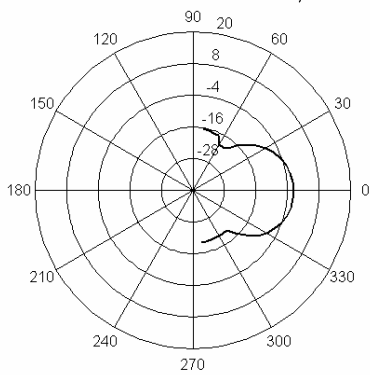
Azimuth (H plane)

Realized Gain at 2000 MHz, FH-1E
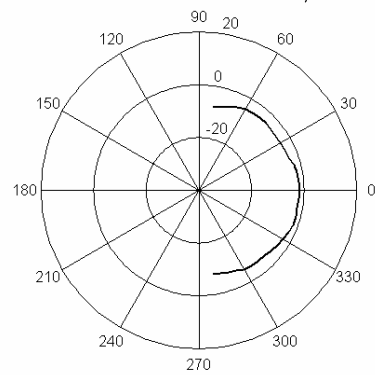
Elevation (E plane)

Realized Gain at 3000 MHz, FH-1E
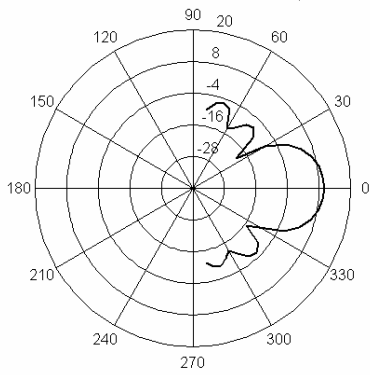
Azimuth (H plane)

Realized Gain at 3000 MHz, FH-1E
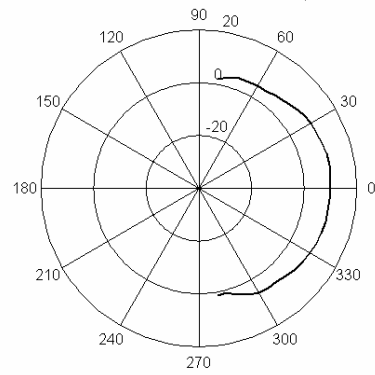
Elevation (E plane)

Figure 6.4 (1 of 2). Pattern plots of the FH-1E folded horn.

Realized Gain at 4000 MHz, FH-1E
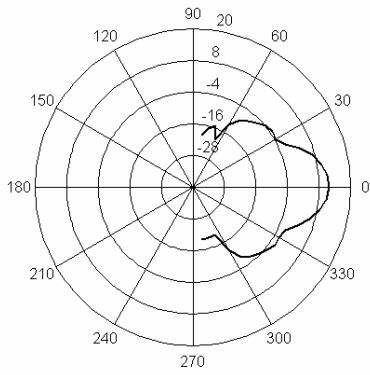
Azimuth (H plane)

Realized Gain at 4000 MHz, FH-1E
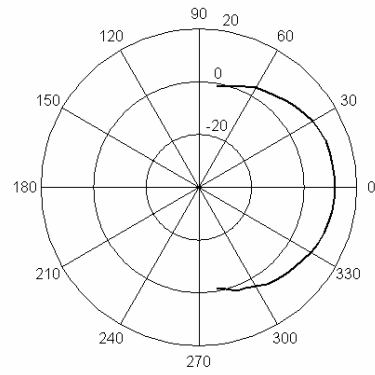
Elevation (E plane)

Realized Gain at 5000 MHz, FH-1E
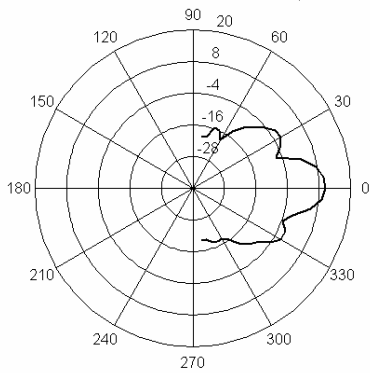
Azimuth (H plane)

Realized Gain at 5000 MHz, FH-1E
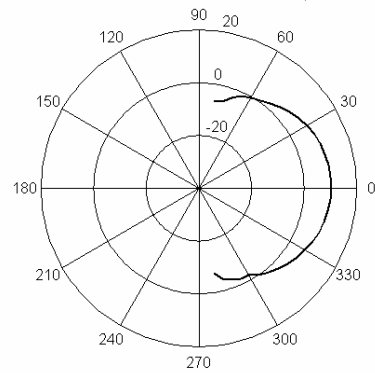
Elevation (E plane)

Realized Gain at 6000 MHz, FH-1E
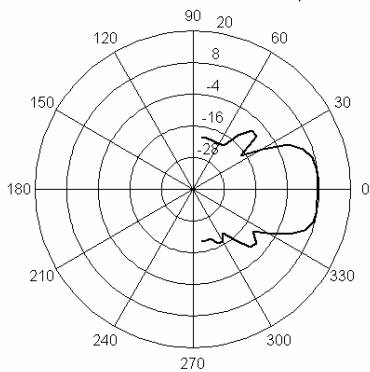
Azimuth (H plane)

Realized Gain at 6000 MHz, FH-1E
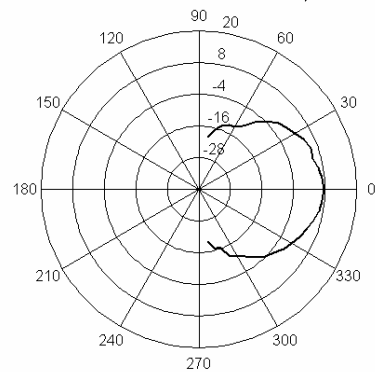
Elevation (E plane)

Figure 6.4 (2 of 2). Pattern plots of the FH-1E folded horn.

VII. FH-1E with Ground Plane

Next, we added a ground plane to the FH-1E, in order to simulate a 2 element array. This configuration might be used if a single switch were used to drive two antennas with equal-but-opposite voltage waveforms. A photo of the FH-1E with ground plane is shown in Figure 7.1, and a sketch of a 2-element array is shown in Figure 7.2.

The TDR and S_{11} of the new configuration are shown in Figure 7.3. We observe minor differences by adding the ground plane, but there are no big changes. The realized gain and antenna patterns are provided in Figures 7.4 and 7.5. Once again, we observe a realized gain of around 10 dB over a frequency range of 3-5 GHz.

Figure 7.1. FH-1E with ground plane.
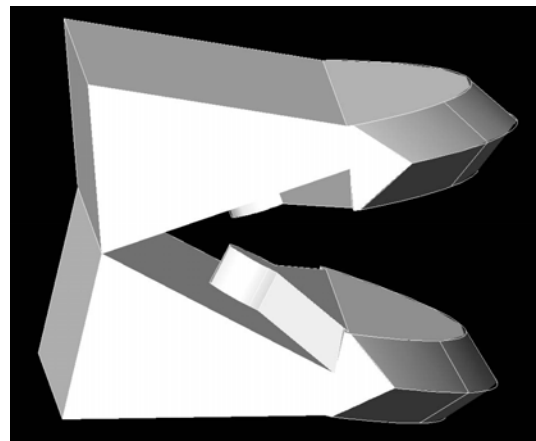
Figure 7.2. A 2-element array of folded horns, which is simulated by a ground plane.
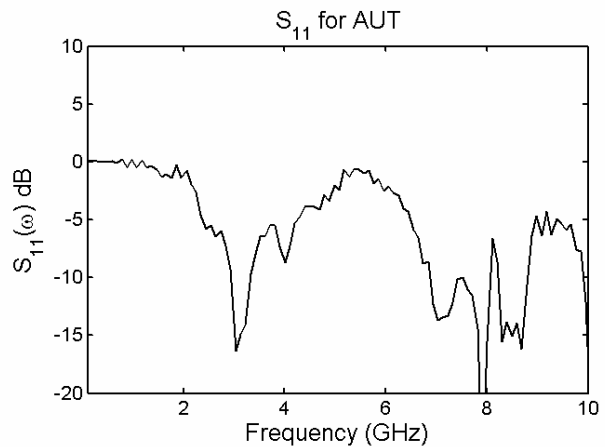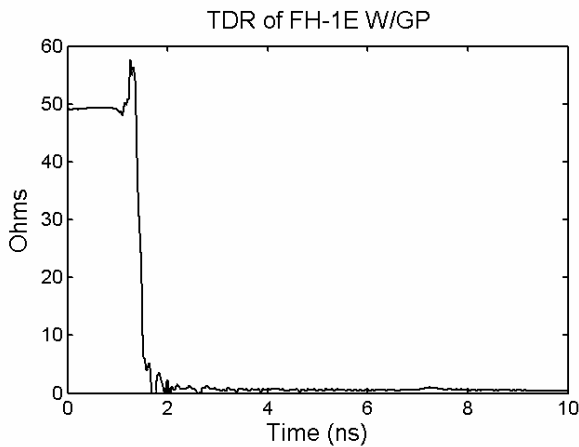
Figure 7.3. TDR and S_{11} of the FH-1E with ground plane.
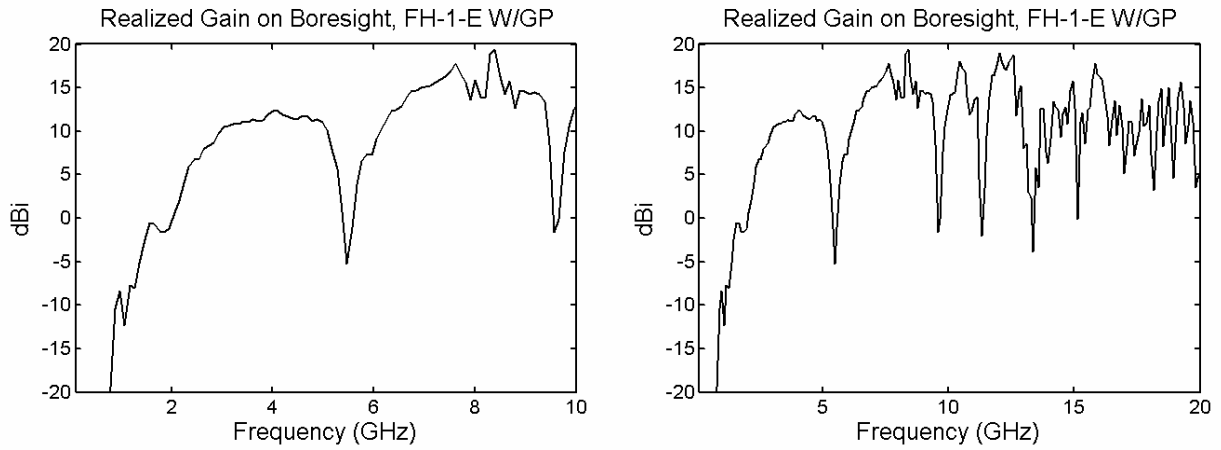
Figure 7.4. Realized gain of the FH-1E with ground plane.
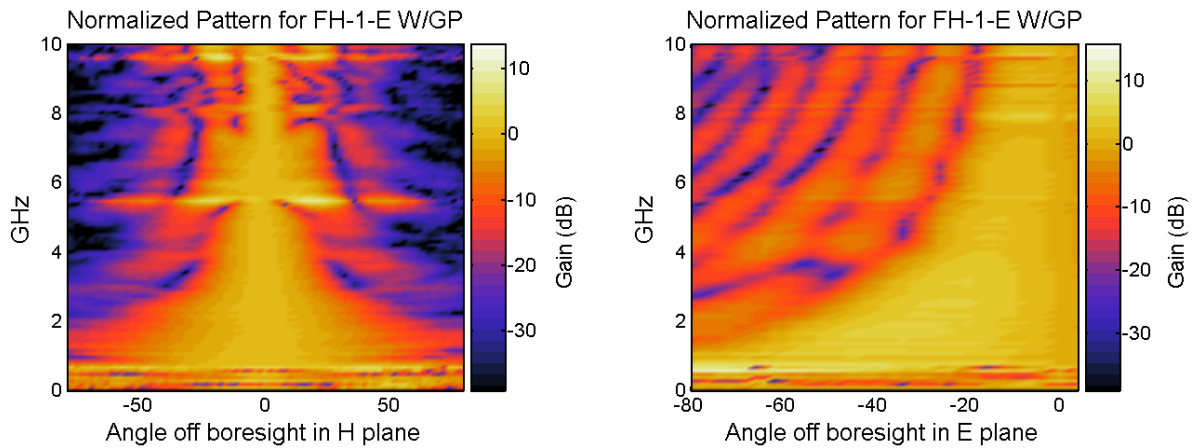
Figure 7.5. Antenna patterns for the FH-1E with ground plane, based on realized gain normalized to boresight.

VIII. Future Improvements

We summarize here the improvements to the folded horn that would be worth exploring.

First, we would like to experiment further with the geometry at the feed point, to further reduce the discontinuities there and to reduce the return loss. These experiments may include varying the radius of the pill box, the angle of the feed cone, and the dielectric constant of the dielectric disk.

Second, we would like to investigate softening the 180° bend in the parabolic reflector, as shown in Figure 8.1. We are concerned that having a sharp knife-edge as shown in the left might introduce ohmic losses and reflection back into the source. It may also cause dielectric breakdown at high voltage.

Figure 8.1. Softening the 180° bend, current design (left) and proposed modification (right).

Third, we would like to investigate the effect of the opening angle of the antenna in the E-plane, θ_E, as shown in Figure 8.2. We have configured the aperture height to be $\lambda/2$, but a larger aperture height might provide even more gain, with little disturbance to the focus in the E-plane.
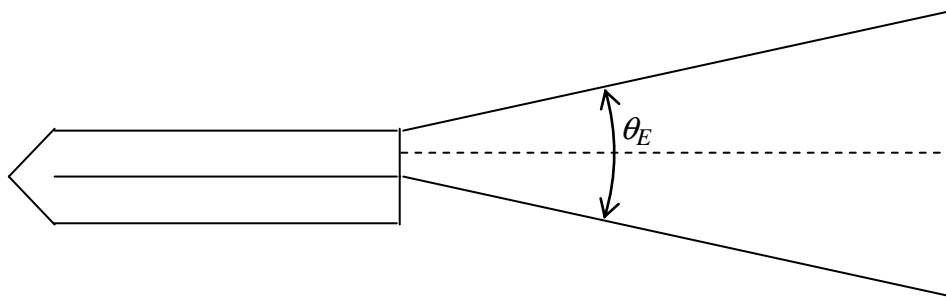
Figure 8.2. Adjusting the opening angle in the E-plane to optimize gain.

Fourth, we would like to investigate bi-folded horn designs, as shown in Figure 8.3. These horns have two folds instead of a single fold. Such designs may be more compact than the single-folded designs. They also allow the possibility of having two sources with equal-but-opposite voltages driving two antennas in parallel.
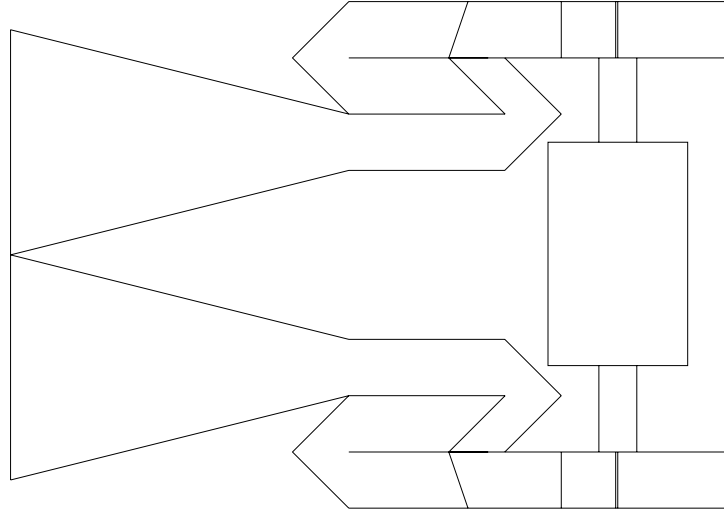
Figure 8.3. Two bi-folded horns, positioned with a source that provides two equal-but-opposite outputs signals.

Finally, we note that all of the above ideas could be tested at low voltage. However, we will ultimately need to incorporate the best design ideas into a large high-voltage version of the antenna.

IX. Conclusions

We have built and tested a folded horn, which is a compact antenna with moderate gain. After a number of iterations, we achieved a realized gain of 10 dB at 3 GHz, which was quite close to our predictions.

A number of areas are worth investigating in the future to improve the folded horn, as described in Section VIII. These include investigations on the 180° bend, opening angle, and feed point of the horn. Different configurations may be of use, such as the bi-folded horn, with two folds. This configuration may better accommodate a two-horn array with a single high-power source between them. Ultimately, high-power versions will have to be built and tested.

References

1. C. E. Baum, "More Antennas for the Switched Oscillator," Sensor and Simulation Note 493, August 2004.

2. W. L Stutzman and G. A Thiele, *Antenna Theory and Design,* 2nd Edition, Wiley, New York, p. 242, eqn. 6.50.